Atmos. Chem. Phys. Discuss., 2, 1403–1427, 2002
www.atmos-chem-phys.org/acpd/2/1403/


Atmospheric Chemistry and Physics Discussions

# The potential of polarization measurements from space at mm and sub-mm wavelengths for determining cirrus cloud parameters

**J. Miao[1], K.-P. Johnsen[2], S. Buehler[1], and A. Kokhanovsky[1]**

[1]Institute of Environmental Physics, University of Bremen, Germany
[2]GKSS Research Center Geesthacht GmbH, Geesthacht, Germany

Received: 30 August 2002 – Accepted: 16 September 2002 – Published: 19 September 2002

Correspondence to: J. Miao (jmiao@uni-bremen.de)

## Abstract

The millimeter and sub-millimeter waves have been attracting a lot of attention recently in the cloud remote sensing community. This is largely because of its potential use in measuring cirrus cloud parameters with airborne or space-borne radiometers. In this study, we examine the possibility of using polarization measurements in this frequency range to retrieve microphysical parameters of cloud ice particles. By using a simple radiative transfer model, the polarization differences of the brightness temperatures measured at the vertical and horizontal polarization channels are calculated at the following seven frequencies: 90, 157, 220, 340, 463, 683, and 874 GHz. The cirrus clouds are modeled with nearly spherical particles, circular cylinder, and circular plate, as well as with mixtures of these types. We found that the polarization difference shows a unique "resonance" feature with the change of ice particle characteristic size: it has a strong response only in a certain range of ice particle size, beyond that range it approaches zero. The size range where this resonance happens depends to a large extent on particle shape and aspect ratio, but to a much less extent on particle orientation. This resonance feature remains even when the particles are mixed with different shapes, although the magnitude and the position of the resonance peak may change, depending on how ice particles are mixed. Oriented particles generally show larger polarization difference than randomly oriented ones, and plates have larger polarization difference than cylinders. However, particle orientations have a significantly stronger influence on the polarization difference than particle shapes (cylinder or plate). This makes it difficult to distinguish particle shapes using millimeter and sub-millimeter radiometric measurements, if there is no information available on particle orientations. However, if the state of particle shape mixture can be predetermined by other approaches, polarization measurements can help to determine ice particle characteristic size and orientation. This information, in turn, will benefit the retrieval of cloud ice water path.



ACPD

2, 1403–1427, 2002

## 1. Introduction

In the last two decades many studies have been carried out for the remote sensing of cirrus clouds from ground, airplane, and satellites (Lynch et al., 2002). Both active and passive approaches have been used. Most of them are exploiting the advantages of the visible, infrared, and microwave range of the electromagnetic spectrum. Recently, the millimeter (mm) and sub-millimeter (sub-mm) wave range, which covers frequencies from about 150 to about 1000 GHz with corresponding wavelength ranging from 2.0 to 0.3 mm, has attracted a great deal of attention. Theoretical simulations as well as experimental studies have been conducted, showing that this spectral range could be very promising in measuring cloud parameters such as the ice water path (IWP) and the ice particle characteristic size (Evans et al., 1998; Wang et al., 2001).

The mm and sub-mm range shows some important advantages compared with the other commonly used spectral ranges. First of all, the wavelengths in this range are comparable with or larger than the sizes of most ice particles. Secondly, the imaginary part of the refractive index of pristine ice in the mm and sub-mm spectrum is much smaller than the real part of the refractive index. These two factors combined cause the interaction between ice particles and the atmospheric radiation to be dominated by the scattering effect, which is almost independent of the ambient temperature of the cloud and only proportional to the volume (or mass) of the ice particles. Furthermore, because of the strong absorption of atmospheric water vapor, the ground surface is almost undetectable for a space-borne mm and sub-mm radiometer. Finally, since cirrus clouds are mostly thin, the brightness temperature depressions induced by cloud ice particle scattering are, in most cases, proportional to the cloud IWP, at these frequencies (Liu and Curry, 2000). This will significantly simplify the retrieval of cloud parameters from radiometric measurements.

However, until now most studies are concerned with the information content of radiometric intensity signals (Evans et al., 1998; Wang et al., 2001). There is a general lack on the study of the potential of polarization measurements in the mm and sub-mm wave



ACPD
2, 1403–1427, 2002

band. In this paper, we will treat this topic in some detail. As mentioned earlier, the ground surface is mostly undetectable for a space-borne mm and sub-mm radiometer, therefore the polarization signal is exclusively caused by the scattering of the unpolarized atmospheric radiation through frozen hydrometeors. By using a simple physical model, we demonstrate in Sect. 2 the advantages of polarization measurements. In Sect. 3 we apply this model to examine the factors influencing the polarization signature as measured by a space-borne mm and sub-mm radiometer. These factors include particle shape, particle orientation, and particle size. And finally, we presents some discussions in Sect. 4 and conclude the paper.

## 2. The physical model

The polarization signature is described by the brightness temperature difference measured by a radiometer at two orthogonally polarized channels, i.e. the vertical and horizontal channels. Highly accurate polarization difference measurements at the microwave band can be achieved with today's technology (Hollinger et al., 1990). The usage of this signature has been shown to be very effective, e.g. in determining surface features as sea ice concentration (Kern and Heygster, 2001) or atmospheric parameters such as rain rate over land (Spencer et al., 1989) and cloud liquid water over sea ice (Miao et al., 2000), by using the Special Sensor Microwave/Imager (SSM/I). Polarization measurements can also be taken with high accuracy at the mm and sub/mm frequencies. To have a general understanding of the information content of the polarization signature of cirrus clouds, we use the simple physical model, as shown in Fig. 1, to describe our problem.

In this simple model, the atmosphere is assumed to be in a plane-parallel structure containing only one single layer of ice cloud. The atmosphere has three layers, which are assumed to be homogeneous and isothermal. Only the middle layer contains ice particles. The brightness temperature observed by a space-borne radiometer at the polarization state $\beta$ is denoted by $T_{b\beta}$ and $\beta$ can be $v$ or $h$, for vertical or horizontal



ACPD
2, 1403–1427, 2002

polarization, respectively. $T_{b\beta}$ can be expressed explicitly by using the physical parameters given for each layer. The reflection and refraction effects at layer boundaries are neglected. Within the cloud layer only single scattering effects are considered for the interaction between ice particles and atmospheric radiation. Under these conditions, $T_{b\beta}$ consists of the following four parts: the first part, denoted by $T_{b\beta,1}$, is the emission from gases in the uppermost layer. The second part, $T_{b\beta,2}$, is the emission from the layer containing a cloud, which is attenuated by gaseous absorption in the uppermost layer. The third part, $T_{b\beta,3}$, represents the radiation coming from the lowermost layer, which is attenuated by the overlaying two layers through both absorption and scattering. And finally the fourth part, $T_{b\beta,4}$, describes the contribution due to ice particle scattering in the cloud layer. This part is also attenuated by the upper layer absorptions. Summing all these parts up gives

$$T_{b\beta} = T_{b\beta,1} + T_{b\beta,2} + T_{b\beta,3} + T_{b\beta,4} \tag{1}$$

The terms on the right-hand side of Eq. (1) can be expressed as

$$T_{b\beta,1} = T_1(1 - e^{-\tau_{a1}\sec\theta}), \tag{2}$$

$$T_{b\beta,2} = T_2(1 - e^{-\tau_{a2}\sec\theta})e^{-\tau_{a1}\sec\theta}, \tag{3}$$

$$T_{b\beta,3} = T_3(1 - e^{-\tau_{a3}\sec\theta})e^{-(\tau_{a1}+\tau_{a2}+\tau_{s2,\beta})\sec\theta}, \tag{4}$$

and

$$T_{b\beta,4} = T_{s\beta}e^{-\tau_{a1}\sec\theta}. \tag{5}$$

Here $\tau_{ai}$ ($i \in 1, 2, 3$) is the partial opacity of layer $i$ due to absorptions. Theoretically, $\tau_{a2}$ includes the effect of cloud ice particle absorptions and depends consequently on the polarization state. However, since ice absorption in the mm and sub-mm frequency range is very small, we hereby neglect this effect in $\tau_{a2}$. The attenuation caused by ice particle scattering is represented by $\tau_{s2,\beta}$, which depends on the polarization state $\beta$.



ACPD
2, 1403–1427, 2002

The physical temperature of each layer is denoted by $T_i$ with $i \in 1, 2, 3$. $T_{s\beta}$ in Eq. (5) represents the contribution of ice particle scattering of radiation at other directions toward the radiometer observing direction. This term is directly related to ice particle properties as particle number, size, shape, and orientation.

Since the first two parts of $T_{b\beta}$, i.e. $T_{b\beta,1}$ and $T_{b\beta,2}$, do not depend on polarization state, these two terms can be canceled by taking differences of the brightness temperatures measured at two orthogonally polarized channels,

$$Q = T_{bv} - T_{bh}. \tag{6}$$

Then the polarization difference $Q$ is free of atmospheric emissions from the cloud and from the uppermost layer, although the uppermost layer still influences $Q$ through the attenuation. This is because of the term $e^{-\tau_{a1}\sec\theta}$ which is contained in both $T_{b\beta,3}$ and $T_{b\beta,4}$.

By defining $T_L$ as

$$T_{bL} = T_3(1 - e^{-\tau_{a3}\sec\theta}), \tag{7}$$

$Q$ can be explicitly written as

$$Q = T_{bL}e^{-(\tau_{a1}+\tau_{a2})\sec\theta}(e^{-\tau_{s2,v}\sec\theta} - e^{-\tau_{s2,h}\sec\theta}) + (T_{sv} - T_{sh})e^{-\tau_{a1}\sec\theta}. \tag{8}$$

The righthand side of the above equation shows that $Q$ consists of two terms describing the contributions from two different sources. The first term represents the direct contribution of the radiation coming from the lowermost layer and traveling through the cloud and the uppermost layer up to the space-borne radiometer. Since the radiation from the lowermost layer is unpolarized, the polarization difference is exclusively induced by the different scattering efficiencies of ice particles at the two different polarization states. The second term, in contrast, expresses the contributions of ice particle scattering. The first term will be zero if ice particles are spherical or randomly oriented,



ACPD
2, 1403–1427, 2002

because, in this case, $\tau_{s2,v}$ and $\tau_{s2,h}$ will be equal. However, the second term generally remains nonzero.

Suppose two different frequencies, $f_1$ and $f_2$, are selected to have the same atmospheric absorption, i.e. $\tau_{ai}(f_1)$ is equal to $\tau_{ai}(f_2)$ for the three layers ($i \in 1, 2, 3$), then the ratio of the two brightness temperature differences $\frac{Q(f_1)}{Q(f_2)}$ will be free of the screening effect (of both emission and attenuation) of the upper layer. This becomes true, because the two terms on the righthand side of Eq. (8) contain a common factor $e^{-\tau_{a1}\sec\theta}$. Furthermore, since $Q$ is proportional to the radiation coming from the lowermost layer, the ratio of the polarization differences at the two frequencies is, to some extent, independent of the atmospheric conditions below the cloud. This will simplify consequent cloud parameter retrievals. Based on this idea, a recently proposed concept of a space-borne mm and sub-mm radiometer, which is dedicated to cirrus cloud measurements, selected some well-matched frequencies (Miao et al., 2002).

Simultaneous measurements at two or more frequencies will enable us to cover a large range of clouds with different particle sizes and optical depths. On the other hand, for thin cirrus clouds polarization difference $Q$ has a linear relationship with the cloud IWP. In this case, polarization measurements at two frequencies can help, to some extent, to get rid of the influence of IWP on $Q$ and to further isolate the information of ice particle microphysical properties. This microphysical property information, when it is available, will further help to retrieve the cloud IWP.

## 3. The information content of polarization measurements

### 3.1. The radiative transfer model

From the physical analysis given in the preceding section, we know that the uppermost layer plays a minor role in the polarization signature analysis. Therefore we neglect the effect of the uppermost layer in the following discussion. By further assuming the cloud layer to be thin and omitting the absorption in this layer, we get a simpler form of



ACPD
2, 1403–1427, 2002

Eq. (8)

$$Q = Q_s + T_{bL}(e^{-\tau_{s2,v}\sec\theta} - e^{-\tau_{s2,h}\sec\theta}), \quad (9)$$

where $Q_s = T_{sv} - T_{sh}$. We get in the single scattering approximation (Mishchenko et al., 2000),

$$Q_s(\boldsymbol{n}) = n_0 \int_{4\pi} \langle Z_{21}(\boldsymbol{n}, \boldsymbol{n}')\rangle I_{in}(\boldsymbol{n}')d\Omega'. \quad (10)$$

Here, $\boldsymbol{n}$ and $\boldsymbol{n}'$ denote the directions of the satellite observation and the incident radiation, respectively. $\langle Z_{21}(\boldsymbol{n}, \boldsymbol{n}')\rangle$ is the element (2,1) of $\langle \mathbf{Z}(\boldsymbol{n}, \boldsymbol{n}')\rangle$, which is the ensemble-averaged phase matrix according to ice particle size, shape, and orientation distributions. $n_0$ is the number density of ice particles in the cloud. $I_{in}(\boldsymbol{n}')$ represents the intensity of radiation incident on the particle from a direction $\boldsymbol{n}'$.

To make the simulation more close to reality, instead of using the isothermal and homogeneous atmosphere in the physical model in the preceding section, we did our simulation for a typical mid-latitude case, using the temperature and humidity profiles (with a surface relative humidity of 80%) of the standard US atmosphere (1976) (Ulaby et al., 1981). The ground surface temperature is set to be equal to the surface air temperature and the surface emissivity is assumed to be 1. The surface emissivity is relatively arbitrary, since the ground surface is undetectable at most of the frequencies considered in this study. The thin cirrus cloud layer is placed at the altitude of 10 km. The satellite observation angle $\theta$ is fixed at 54°. $T_{bL}$ and $I_{in}(\boldsymbol{n}')$ are calculated using the radiative transfer model described by Gasiewski (1993). Since the atmosphere is taken to be plane-parallel, the intensity of the incident radiation, $I_{in}(\boldsymbol{n}')$, depends only on the incidence angle. At the altitude of 10 km the radiation coming from the lower atmosphere (>230 K) is much stronger than from the upper atmosphere (a few tens of Kelvin) at the frequencies considered in this paper.



ACPD
2, 1403–1427, 2002

### 3.2. The microphysical model

In situ measurements have shown that cirrus clouds are usually composed of non-spherical ice particles (McFarquhar and Heymsfield, 1996). For our simulations we selected three types of particles: nearly spherical particles, circular cylinder, and circular plates. Ice particles are treated as pristine ice crystals with a density of 0.92 g cm$^{-3}$. The particle size is sorted with its maximum dimension, which is the length for cylinders and the diameter for plates. For nearly spherical particles, the diameter of the mass equivalent sphere is used to define the particle size. In this paper, the maximum particle size is taken to be 2.0 mm and the minimum is 20 $\mu$m. This range of particle size is reasonable becasue, although there may exits a large number of smaller ice particle in realistic cirrus clouds (Lin et al., 1998), they are not significant enough for mm and sub-mm wave scattering due to the very small volume fraction of this knid of ice particles in clouds. The particle size distribution is assumed to be

$$N(D) = aD^{\alpha} e^{-\frac{\alpha+3.67}{D_m}D}, \tag{11}$$

where $a$ is a constant and $\alpha$ is the width parameter usually ranging from 0 to 2 (Evans et al., 1998). Parameter $D_m$ is the median of the distribution of $D$ to the third power, which means, the total mass of ice particles of sizes from zero to $D_M$ is equal to that from $D_m$ to infinity. Since the distribution is truncated at 2.0 mm of $D$, there will be a mass loss for the part with sizes larger than $D_m$. This mass loss will increase with $D_m$. Our calculations show that, for $\alpha = 1$, the mass loss is 1% of the total mass when $D_m$ equals 0.8 mm. This loss increases to ~4% when $D_m$ increases to 1.0 mm. Since the width parameter $\alpha$ was found to play a minor role in the particle scattering properties, the following discussions are exclusively limited to cases with $\alpha = 1$ (Lemke and Quante, 1999).

To calculate the single scattering parameters of ice particles, i.e. $\tau_{s2,\beta}$ ($= n_0\langle C_{sca,\beta}\rangle$) and $\langle Z_{21}(\boldsymbol{n}, \boldsymbol{n}')\rangle$, the T-Matrix method and the Discrete Dipole Approximation (DDA) method are used (Mishchenko and Travis, 1998; Draine and Flatau, 1998). $\langle C_{sca,\beta}\rangle$



ACPD
2, 1403–1427, 2002

is the ensemble-averaged scattering cross section of a single ice particle, based on a given size, shape and orientation distribution. Because the T-Matrix method has a high computational efficiency, it is used for the calculation of single scattering parameters of most particles used in this study. However, there are cases when the particle size as well as aspect ratio is large and convergence fails to achieve. Then, the DDA method, due to its flexibility and robustness, will be used. The single scattering properties of nearly spherical particles are represented by an average of those from spheroid (both prolate and oblate), circular cylinders and circular plates with aspect ratios $\eta$ less than 1.5. $\eta$ denotes the ratio of the maximum to the minimum dimension of a non-spherical particle. In situ observations found that ice particle ratios can change from 1 to 7 for cylinders and from 5 to 30 for plates (Auer and Veal, 1970). Our simulations for circular cylinder were done for aspect ration from 1 to 7 and for circular cylinder of 1, 3, 5, 10, 20, and 30. The frequencies used are 90, 157, 220, 340, 463, 683, and 874 GHz. Among these frequencies some (90, 157, 220, and 340 GHz) have been tested in space-borne or air-borne sensors and some (463, 683, and 874 GHz) are found to be well matched in atmospheric absorption and have been included in a new satellite mm/sub-mm radiometer concept (Miao et al., 2002). The refractive index of pristine ice at the used frequencies is given in Table 1, which is taken from the data set given by Warren (1984) and for a specific ambient temperature of 250 K.

### 3.3. The information content of the polarization signature

#### 3.3.1. Clouds with randomly oriented ice particles

In this section, we consider ice clouds composed of randomly oriented ice particles. Although aerodynamic and gravitational forces tend to cause ice needles and plates, especially those with large size and aspect ratio, to have a preferred horizontal orientation for their longer axes (Brussaard and Watson, 1995), the orientation angle distribution for the whole ensemble of ice crystals changes from case to case (Chepfer et al., 1999). Therefore, random orientation is often a good approximation to the simulation



ACPD
2, 1403–1427, 2002

of single scattering properties of cirrus cloud ice particles and for the retrieval of cirrus cloud parameters such as particle shape and IWP (Baran et al., 2001; Chepfer et al., 2001). For random orientation, $\tau_{s2,v}$ is equal to $\tau_{s2,h}$, causing the second term on the righthand side of Eq. (9) to vanish.

In Fig. 2 the simulated polarization difference $Q$ is shown versus the diameter of the median mass equivalent sphere for the case of nearly spherical particles. Results are given for all 7 frequencies mentioned in the preceeding section. The cirrus cloud is assumed to have an ice water path of 60 $\mathrm{gm}^{-2}$, which becomes 100 $\mathrm{gm}^{-2}$ along the slant satellite observation line. Since only single scattering effect is considered in the radiative transfer within the cirrus cloud, the simulation results given here can only be quantitatively used for thin clouds. Therefore, the values of the polarization difference $Q$ given in Fig. 2 and in the following Figs. 3, 4, and 6 should be taken as the value per 60 $\mathrm{gm}^{-2}$ of cloud IWP, when cloud IWP is other than 60 $\mathrm{gm}^{-2}$.

It follows from Fig. 2 that, for a given frequency, $Q$ is only sensitive to ice particles within a certain range of sizes. This feature can be called a "resonance". The magnitude of the resonance peak of $Q$ increases with increasing frequency $f$. The peak position $D_m^*$ also changes with frequency: the ratio of $D_m^*$ and wavelength $\lambda$ remains nearly constant (= 0.4). This feature tells us that high frequencies are more sensitive to smaller particles and lower frequencies are more sensitive to larger particles. Especially, when particle characteristic size $D_m$ is less than ~120 $\mu$m, there exists a monotonic relationship between the polarization difference $Q$ and frequency $f$. Consequently, multi-frequency measurements of the polarization difference $Q$ are potentially useful in determining ice particle characteristic size of cirrus clouds. However, this conclusion is limited to clouds with nearly spherical particles in random orientation.

If cirrus clouds are composed of other forms of particles, the results will be somewhat different. In Fig. 3 simulated polarization differences for circular cylinders are shown versus particle characteristic size. These are results for a fixed frequency (683 GHz) but with changing particle aspect ratio. Clearly, the aspect ratio of the particles here plays a crucial role in the relations between the polarization difference $Q$ and the parti-



ACPD
2, 1403–1427, 2002

cle size $D_m$. With the increase of particle aspect ratio, the magnitude of the resonance peak increases and the position of the peak moves toward large particles. When $D_m$ is less than ~150 $\mu$m, $Q$ is inversely proportional to the aspect ratio, while for $D_m$ larger than ~700 $\mu$m, $Q$ becomes directly proportional to the aspect ratio. Simulations for circular plates show similar results (Fig. 4). However, difference is obvious in the following two aspects compared with circular cylinder case. First, the position of the resonance peak moves much more slowly with increasing particle aspect ratio for the case of plates. Secondly, the magnitude of the resonance peak decreases slightly when aspect ratio of plates changes from 20 to 30. This phenonenon does not appear for cylinders with aspect ratios less than 7. However, the two ranges of $D_m$, where monotonic relationship appears between polarization difference and aspect ratio, are nearly identical for the two types of particles.

#### 3.3.2. Effects of particle's orientations and shape mixtures

Natural ice clouds are a mixture of irregular ice particles with differing shapes and orentations. In this section we present two simple examples, in order to examine how these factors affect the polarization difference.

In examining particle orientation effect, we follow the procedure of Aydin and Tang (1997). Ice particles are assumed to be in simple forms, circular cylinder and circular plate, with the same aspect ratio. We assume that they have a preferred orientation angle relative to the horizontal plane but the particle axis is in a uniform distribution in the azimuth. The orientation angle $\delta$ is the angle formed by the axis of the largest dimension of the particle and the horizontal plane. For our simulations, orientation angle $\delta$ follows the truncated Gaussian function,

$$p(\delta) = \frac{1}{C_0} e^{-(\delta-\bar{\delta})^2/2{\sigma_\delta}^2}, \tag{12}$$

with

$$C_0 = \int_0^{\pi/2} e^{-(\delta-\bar{\delta})^2/2{\sigma_\delta}^2} \sin\delta d\delta. \quad (13)$$

$\delta$ changes in the range of $[0, \pi/2]$. If $\bar{\delta}$ is zero, then the average orientation of ice particles lies in the horizontal plane. Note, $\int_0^{\pi/2} p(\delta)\sin\delta d\delta = 1$.

Our simulations show that, when particles are oriented, the polarization difference $Q$ is generally larger than in the case of a random orientation. Especially, when $\sigma_\delta$ is zero, i.e. all particles are horizontally oriented, the peak value of $Q$ is several times larger than that at a random orientation: 8 times for cylinders and over 10 times for plates (see Fig. 5a and b). In general, orientation has a larger effect on plates than on cylinders. However, with the increase of width parameter $\sigma_\delta$, $Q$ decreases rapidly. When $\sigma_\delta$ equals 30°, the peak of $Q$ is already less than 50% of the value for the case of $\sigma_\delta = 0$. This is true for cylinders as well as for plates. It is noteworthy that the peak position of $Q$ in particle characteristic size $D_m$ changes little for plates when the orientation width parameter $\sigma_\delta$ changes from zero to infinity. For cylinders, however, the peak position of $Q$ initially remains nearly unchanged as $\sigma_\delta$ increases from zero to 20°. As $\sigma_\delta$ approaches infinity from 20°, the peak position moves gradually from $\sim 500\,\mu$m to $\sim 600\,\mu$m in $D_m$. Based on this simulation, we state that the resonance feature of the polarization difference $Q$ with respect to frequency, particle aspect ratio, and particle characteristic size, which was found for the randomly oriented particles, remains similar for oriented particles, with the exception that the magnitude of the resonance peak increases dramatically when ice particle orientations change gradually from random to fully horizontal. We also noticed that particle orientation has a much more prominent effect than particle shape to the magnitude of the resonance peak (compare Figs. 5a and 5b).

The effect of particle shape mixture is shown in Fig. 6 by the simulation results done for merely circular cylinders. In this simulation, we assume ice particle numbers to be still in a modified Gamma distribution in respect to particle siae, as given in Eq. (1).



ACPD
2, 1403–1427, 2002

However, ice particles at a certain size (i.e. the length of the circular cylinder) are composed of cylinders having equal lengths but with differing aspect ratios. The number fraction of ice particles in each aspect ratio is described by a discrete, truncated Gaussian function,

$$g(\eta) = \frac{1}{D_0} e^{-(\eta-\bar{\eta})^2/2{\sigma_\eta}^2}. \quad (14)$$

$\eta$ denotes aspect ratio and takes discrete values from 1 to 7. $D_0$ is a normalization constant, enabling $\sum_{\eta=1}^{7} g(\eta) = 1$. The average aspect ratio $\bar{\eta}$ changes linearly with particle length, changing from 1 to 7 as the cylinder length increases from zero to 2.0 mm. The degree of shape mixture is controlled by the width parameter $\sigma_\eta$. Apparently, when $\sigma_\eta$ is small, the particles at a certain length are composed mainly by cylinders with an aspect ratio corresponding to that length according to the linear relationship between $\bar{\eta}$ and particle length. When $\sigma_\eta$ becomes larger and finally approaches infinity, particles will be composed of equal portions of cylinders with aspect ratio from 1 to 7.

The results in Fig. 6 show that shape mixture has an influences both on the magnitude and on the position of the resonance peak of the polarization difference $Q$. Compared with the results for cylinders with the same aspect ratio, $Q$ shows a considerably higher wing in the right side extending to large particle sizes. With an increasing width parameter $\sigma_\eta$, the polarization difference $Q$ approaches that of the case with a small but fixed aspect ratio (compare Fig. 3). This is understandable. Since the volume of a cylinder with smaller aspect ratio is much larger than that of a cylinder in the same length but with a larger aspect ratio, particles with small aspect ratio will gradually dominate the volume of the ice particle ensemble, with the increase of the width parameter $\sigma_\delta$. As a result, they will also gradually dominate the scattering effect.

Although shape mixture has a considerable influence on the polarization difference $Q$, the basic feature $Q$ in respect to particle characteristic size does not change. We mean that the polarization difference measured at a given frequency still shows its resonance for particles at a certain range of sizes, even though particles are a mixture of different shapes.

## 4. Conclusions

The main purpose of this study is to promote a general understanding of the potential of polarization measurements from space at mm/sub-mm wavelengths in determining cirrus clouds parameters but not to quantify the polarization signature for realistic cirrus clouds. To this end, simplified radiative transfer procedures have been pursued, which include (1) using single scattering to describe the interaction of the ice particles and atmospheric radiation; (2) ignoring the water vapor screening effect in the layers above the clouds; and (3) using circular cylinders, circular plates and nearly spherical particles to simulate natural ice particles.

Despite the simplifications introduced in the simulations, our results clearly show the unique features of polarization measurements. The most outstanding one is the resonance of the polarization difference for ice particles in a certain range of sizes. This resonance feature is also reported recently in a simulation and measurement study by Troitsky et al. (2001) for precipitating clouds at lower frequencies (<85 GHz). Furthermore, we found that the resonance peak in respect to particle size changes from large to small when the observing frequency increases from low to high. The position of resonance peak depends also on the particle shape and the aspect ratio. This resonance feature appears even when the particles are oriented or mixed with different shapes, although the exact magnitude and position of the resonance peak may change accordingly. The unique features of polarization difference with respect to particle microphysical properties found in this study suggest that polarization measurements from satellite at some well-chosen mm/sub-mm frequencies will benefit the determination of cirrus cloud parameters. And, polarization measurements in mm and sub-mm wavelength are also an excellent complement to similar measurements in infrared and visible wavelength in determining microphysical properties of a wide range of cirrus clouds (Liou and Takano, 2002).

Caution must be taken when trying to compare measurements with the simulation results given in this study, especially when ice clouds are optically thick. Since multiple



ACPD
2, 1403–1427, 2002

scattering has not been considered in the radiative transfer calculations, our simulation results are limited to optically thin clouds. For example, at 683 GHz an ice cloud with an IWP of 6 $gm^{-2}$ has an optical depth of <0.1, if the cloud is composed of circular ice cylinders with aspect ratio of 5 and median mass length of 500 $\mu$m. The single scattering radiative transfer can be taken to be valid for this case, then the polarization difference measured by a space-borne radiometer ranges from a few tenths of a Kelvin for randomly oriented particles to a few Kelvin for fully horizontally oriented particles (referring to Fig. 5a). The screening effect of the atmosphere in the top layer above the cloud is negligible in this specific case, since the transmission of the this layer at the highest frequencies used in this study is larger than 0.95.

Future work will be focused on the quantitative determination of the polarization difference for various ice clouds composed of more realistic ice particles. Especially, the multiple scattering effect and the inhomogeneity in both horizontal and vertical dimensions of the cloud will be taken into account. For this purpose, a three-dimensional, fully-polarized radiative transfer model is under development in the Institute of Environmental Physics, University of Bremen (Kerridge et al., 2002). A cloud parameter retrieval scheme taking into account of the polarization measurements will also be developed.

*Acknowledgements.* This study was supported by the German AFO 2000 research program under grant 07ATC04 (Project UTH-MOS) and in part by the European Union under contract ENV4-CT98-0733.

## References

Auer, A. H. and Veal, D. L.: The dimensions of ice crystals in natural clouds, J. Atmos. Sci., 27, 919–926, 1970. 1412

Aydin, K. and Tang, C.: Millimeter wave radar scattering from model ice crystal distribution, IEEE Trans. Geosci. Remote Sensing, 35, 140–146, 1997. 1414

Baran, A. J., Francis, P. N., Havemann, S., and Yang, P.: A study of the absorption and extinction properties of hexagonal ice columns and plates in random and preferred orientation,

using exact T-matrix theory and aircraft observations of cirrus, J. Quant. Spectrosc. Radiat. Transfer, 70, 505–518, 2001. 1413

Brussaard G. and Watson, P. A: Atmospheric modelling and millimetre wave propagation, Chapman & Hall, London, UK, 1995. 1412

Chepfer, H., Brogniez, G., Goloub, P., Breon, F. M., and Flamant, P. H.: Observation of horizontally oriented ice crystals in cirrus clouds with POLDER-1/ADEOS-1, J. Quant. Spectrosc. Radiat. Transfer, 63, 521–543, 1999. 1412

Chepfer, H., Goloub, P., Riedi, J., DeHaan, J. F., Hovenier, J. W., and Flamant, P. H.: Ice crystal shapes in cirrus clouds derived from POLDER-1/ADEOS-1, J. Geophys. Res., 106, 7955–7966, 2001. 1413

Draine, B. T. and Flatau, P.: User guide for the discrete dipole approximation code DDSCAT (Version 5a10), J Princeton Observatory Preprint POPe-xxx, 1998. 1411

Evans, K. F., Walter, S. J., Heymsfield, A. J., and Deeter, M. N.: Modeling of submillimeter passive remote sensing of cirrus clouds, J. Atmos. Sci., 37, 184–205, 1998. 1405, 1411

Gasiewski, A. J.: Microwave radiative transfer in hydrometeors, Atmospheric remote sensing by microwave radiometry, (Ed) Janssen, M. A., John Willy & Sons, Inc., pp. 91–144, 1993. 1410

Hollinger, J. P., Peirce, J. L., and Poe, G. A.: SSM/I instrument evaluation, IEEE Trans. Geosci. Remote Sensing, 28, 781–789, 1990. 1406

Kern, S. and Heygster, G.: Sea-ice concentration retrieval in the Antarctic based on the SSM/I 85.5 GHz polarization, Annals of Glaciology, 33, 109–114, 2001. 1406

Kerridge, B., Siddans, R., Latter, B., Dudhia, A., Lama, F., Stiller, G., v. Clarmann, T., Grabowski, U., Buehler, S., Miao, J., Emde, C., Murtagh, D., Eriksson, P., Lary, D., Mussa, H., Lee, A., and Baran, A.: Consideration of mission studying: Chemistry of the UTLS, Progress Report 2, ESTEC Contract No 15457/01/NL/MM, 2002. 1418

Lemke, H. M. and Quante, M.: Backscatter characteristics of nonspherical ice crystals: Assessing the potential of polarimetric radar measurement, J. Geophys. Res., 104, 31,739–31,751, 1999. 1411

Lin, H., Noone, K. J., Ström, J., and Heymsfield, A. J.: Small ice crystals in cirrus clouds: A model study and comparison with in situ observations, J. Atmos. Sci., 55, 1928–1939, 1998. 1411

Liou, K. N. and Takano, Y.: Interpretation of cirrus cloud polarization measurements from radiative transfer theory, Geophys. Res. Let., 29, 27,1–27,4, 2002. 1417

Liu, G. and Curry, J. A.: Determination of ice water path amd mass median particle size using multichannel microwave measurements, J. Appl. Meteor., 39, 1318–1329, 2000. 1405
Lynch, D. K., Sassen, K., Starr, D. O., and Stephens, G., Cirrus, Oxford University Press, Oxford, 2002. 1405
McFarquhar, G. M. and Heymsfield, A. J.: Microphysical characteristics of three anvils samples during the Central Equatorial Pacific Experiment, J. Atmos. Sci., 53, 2401–2423, 1996. 1411
Miao, J., Johnsen, K.-P., Kern, S., Heygster, G., and Kunzi, K.: Signature of clouds over Antarctic sea ice detected by the Special Sensor Microwave/Imager, IEEE Trans. Geosci. Remote Sensing, 38, 2333–2344, 2000. 1406
Miao, J., Rose, T., Kunzi, K., and Zimmermann, P.: A future millimeter/sub-millimeter radiometer for satellite observation of ice clouds, Int. J. Infrared and Millimeter Waves, 23, 1159–1170, 2002. 1409, 1412
Mishchenko, M. I. and Travis, L.: Capabilities and limitations of a current fortran implementation of the T-Matrix method for randomly oriented, rotationally symmetric scatterers, J. Quant. Spectrosc. Radiat. Transfer, 60, 309–324, 1998. 1411
Mishchenko, M. I., Hovinier, J. W., and Travis, L. D.: Light scattering by nonspherical particles: Theory, measurements, and application, Academic Press, 2000. 1410
Spencer, R. W., Goodman, H. M., and Hood, R. E.: Precipitation retrieval over land with SSM/I: Idenetification of the scattering signal, J. Atmos. Oceanic Technonol., 6, 254–273, 1989. 1406
Troitsky, A. V., Osharin, A. M., Korolev, A. V., Strapp, W., and Isaa, G.: Studying the polarization characteristics of thermal microwave emission from a cloudy atmosphere, Radiophysics and Quantum Electronics, 44, 935–948, 2001. 1417
Ulaby, F. T., Moore, R. K., and Fung, A. K.: Micorwave remote sensing: Active and passive, Artech House, Norwood, MA 02062, 1981. 1410
Wang, J. R., Liu, G., Spinhirne, J. D., Racette, P., and Hart, W. D.: Observation and retrievals of cirrus cloud parameters using multichannel millimeter-wave radiometric measurements, J. Geophys. Res., 106, 15 251–15 263, 2001. 1405
Warren, S. G.: Optical constants of ice from the ultraviolet to the microwave, Appl. Opt., 23, 1206–1223, 1984. 1412



ACPD
2, 1403–1427, 2002

**Table 1.** The refractive index of pristine ice at a temperature of 250 K for some mm and sub-mm frequencies

| f(GHz) | $\lambda$(mm) | Real Part | Imaginary Part |
|---|---|---|---|
| 90 | 3.333 | 1.7823 | 0.0026 |
| 157 | 1.910 | 1.7818 | 0.0039 |
| 220 | 1.364 | 1.7815 | 0.0049 |
| 340 | 0.882 | 1.7815 | 0.0067 |
| 463 | 0.648 | 1.7820 | 0.0084 |
| 683 | 0.439 | 1.7846 | 0.0111 |
| 874 | 0.343 | 1.7895 | 0.0134 |



ACPD
2, 1403–1427, 2002

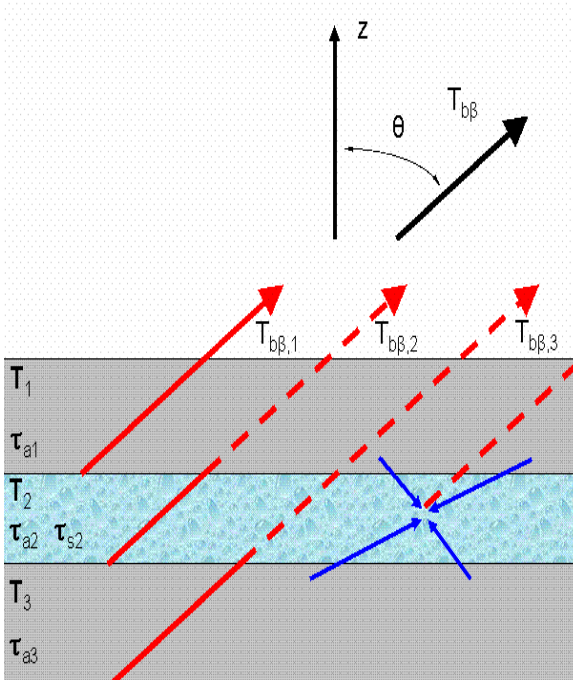


**Fig. 1.** The geometry of the problem.



ACPD
2, 1403–1427, 2002

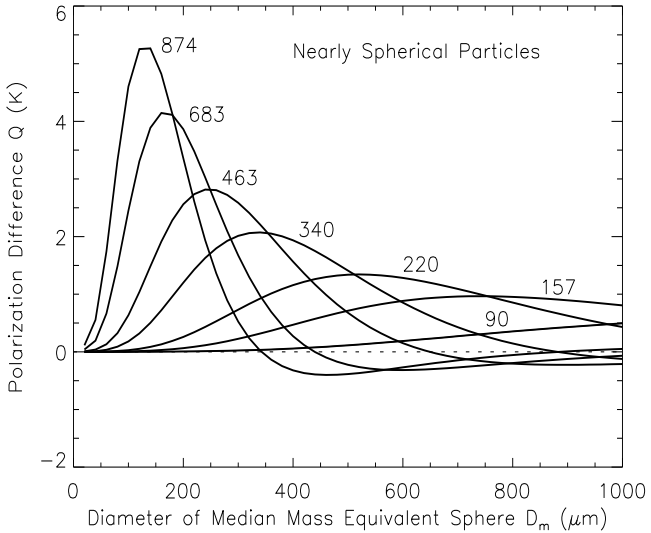


**Fig. 2.** Simulated polarization differences for clouds composed of randomly oriented, nearly spherical particles. Results are shown for all 7 frequencies, which are in GHz and denoted above each curve. Detailed explanations are in the text.



ACPD
2, 1403–1427, 2002

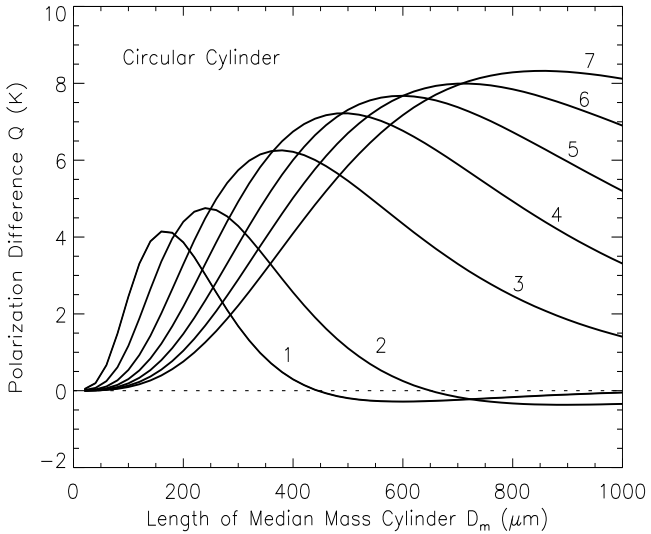


**Fig. 3.** Simulated polarization differences for clouds composed of randomly oriented circular cylinders with differing aspect ratios (denoted close to curves) at 683 GHz. Note, the particle characteristic size $D_m$ represents the length of the median mass cylinder in this case.



ACPD
2, 1403–1427, 2002

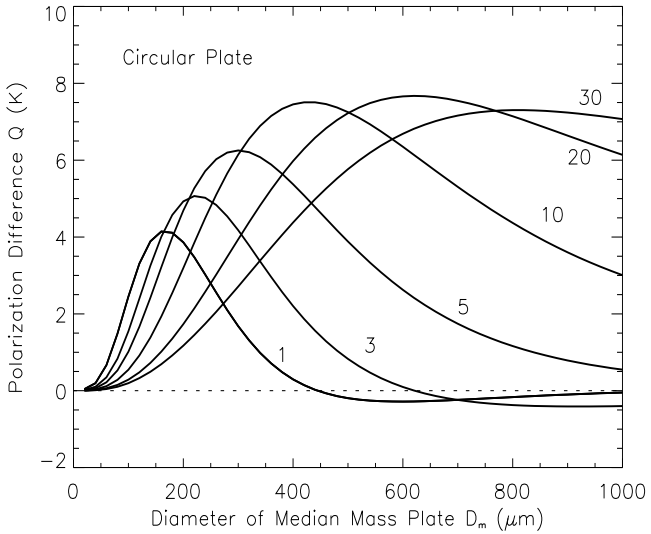


**Fig. 4.** Simulated polarization differences for clouds composed of randomly oriented circular plates with differing aspect ratios (denoted close to the curves) at 683 GHz. Note, the particle characteristic size $D_m$ represents the diameter of the median mass plate in this case.



ACPD
2, 1403–1427, 2002

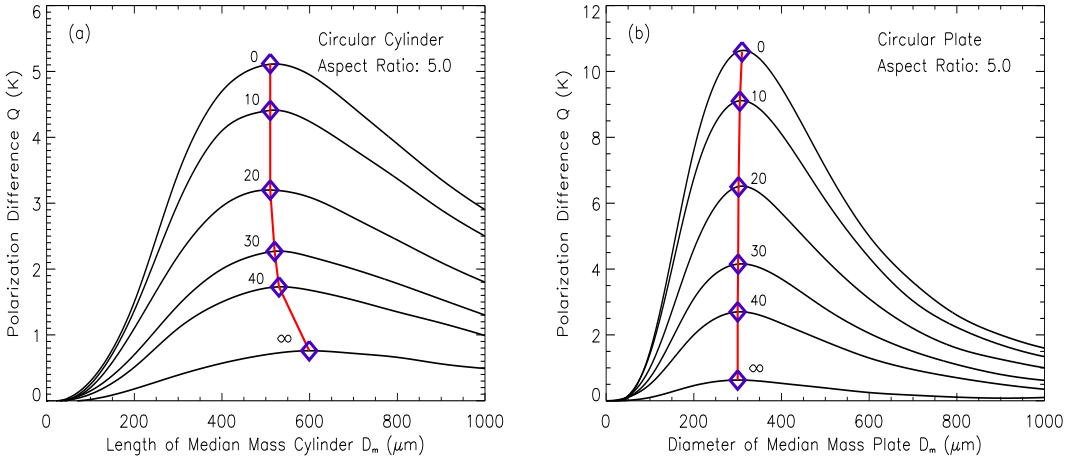


**Fig. 5.** Effect of particle orientation: The particle orientation angle $\delta$ follows a truncated Gaussian function described by Eqs. (12) and (13). The average orientation angle $\bar{\delta}$ is set to zero while the width parameter $\sigma_\delta$ changes from zero to infinity. $\sigma_\delta = 0$ means fully horizontal orientation and $\sigma_\delta = \infty$ means random orientation. The frequency is fixed at 683 GHz. Note, the value of $Q$ shown here represents the polarization difference (in Kelvin) per 6 $gm^{-2}$ of IWP. Diamond marks the position of the resonance peak.



ACPD
2, 1403–1427, 2002

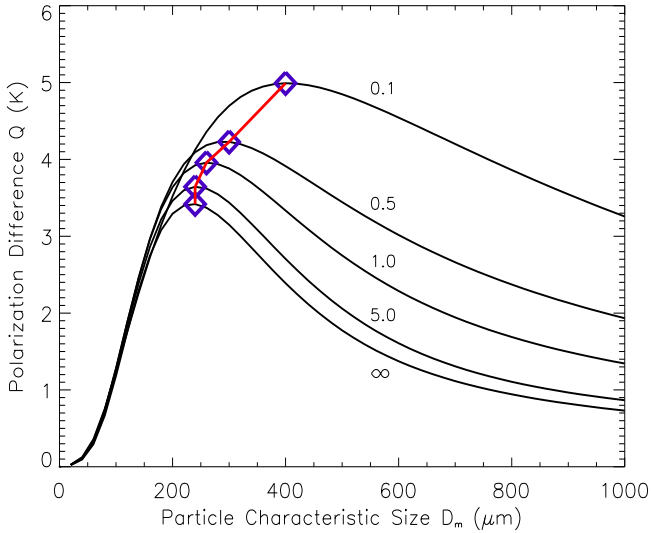


**Fig. 6.** Effect of particle shape mixture: Ice particles are a mixture of cylinders with differing aspect ratio from 1 to 7 and the number of each kind of cylinders is determined using a truncated Gaussian function (see details in text). The results shown correspond to width parameter $\sigma_\eta$ changing from 0.1 to infinity. The frequency is fixed at 683 GHz. Note, $Q$ should be taken as polarization difference (in Kelvin) per 60 $gm^{-2}$ of ice water path. Diamond marks the position of the resonance peak.



ACPD
2, 1403–1427, 2002